

RESEARCH

Open Access



# Impaired hippocampal neurogenesis associated with regulatory ceRNA network in a mouse model of postoperative cognitive dysfunction

Jingrun Lin<sup>1†</sup>, Xiaoqiu Zhu<sup>1†</sup>, Xuan Li<sup>1†</sup>, Yu Hong<sup>1</sup>, Yaohui Liang<sup>2</sup>, Siqi Chen<sup>1</sup>, Chenzhuo Feng<sup>3\*</sup> and Lin Cao<sup>1\*</sup>

## Abstract

**Background** Postoperative cognitive dysfunction (POCD) represents a post-surgical complication that features progressive cognitive impairment and memory loss, often occurring in elderly patients. This study aimed to investigate the potential biological mechanisms underlying POCD.

**Methods** Male C57BL/6 mice (2 and 17 months old) were randomly assigned to surgery or control groups. The surgery group underwent laparotomy under 1.5% isoflurane anesthesia, while controls received no intervention. Cognitive function was assessed 7–10 days post-surgery using open field, Y-maze, and novel object recognition tests.

Hippocampal mRNA expression was analyzed using Encyclopedia of Genes and Genomes (KEGG) and Gene Ontology (GO) enrichment. A competing endogenous RNA (ceRNA) network was constructed using microRNA (miRNA) target prediction databases (miRanda, miRTarbase, miRcode) and sequencing results. Key findings were validated by RT-qPCR and immunofluorescence. The Connectivity Map (CMap) database was queried to predict potential POCD treatments.

**Results** Aging significantly affected mice's spontaneous activity in the open field test ( $F_{1, 28} = 8.933, P < 0.01$ ) and the proportion of time spent in the center area ( $F_{1, 28} = 5.387, P < 0.05$ ). Surgery significantly reduced the rate of spontaneous alternations in the Y-maze ( $F_{1, 28} = 16.94, P < 0.001$ ) and the recognition index in novel object recognition test ( $F_{1, 28} = 6.839, P < 0.05$ ) in aging mice, but had no effect on young mice. Transcriptome analysis revealed that aging and surgery downregulated multiple neurogenesis-related genes in the hippocampus. Doublecortin (DCX) immunofluorescence staining confirmed reduced hippocampal neurogenesis in aging mice, which was further decreased after surgery. We identified several key lncRNAs and miRNAs implicated in neurogenesis regulation. Additionally, drugs were predicted as potential therapeutic candidates for POCD treatment.

**Conclusion** Both aging and surgery have complex effects on the hippocampal transcriptome in mice. The significant decrease in neurogenesis may be a potential reason for the increased susceptibility of aging mice to POCD. The

<sup>†</sup>Jingrun Lin, Xiaoqiu Zhu and Xuan Li contributed equally to this work and share first authorship.

\*Correspondence:

Chenzhuo Feng  
20160030@hmc.edu.cn

Lin Cao  
caolin@mail.sysu.edu.cn

Full list of author information is available at the end of the article



identified key regulatory lncRNAs, miRNAs, and drugs provide potential therapeutic targets for POCD prevention and treatment.

**Keywords** POCD, Aging, lncRNA, miRNA, mRNA, ceRNA, Neurogenesis

## Introduction

POCD is a clinical syndrome with symptoms of memory loss following surgery, including deficits in attention, memory, and information processing capabilities [1]. Longer hospital stays, decreased quality of life, and potentially higher mortality rates are possible outcomes [2]. Additionally, some patients with POCD may progress to permanent dementia, significantly impacting their lives [3]. POCD is more common in elderly persons [4], and as the population ages, the incidence of POCD is expected to rise, further straining healthcare systems [5]. Despite theories implicating amyloid accumulation, tau hyperphosphorylation, and neuroinflammation, the molecular mechanisms driving POCD remain unclear, highlighting the need for further investigation [6–8]. Hence, studying the pathogenic mechanisms of POCD is crucial for gaining new insights that could aid in its prevention and treatment.

Recent advances in molecular biology have revealed that non-coding RNAs play crucial roles in various neurological disorders, providing new perspectives for understanding POCD pathogenesis. lncRNAs are naturally occurring non-coding RNA molecules longer than 200 nucleotides [9]. miRNAs are short single-stranded RNA molecules, typically 21–23 nucleotides long, which regulate gene expression by binding to mRNAs [10]. lncRNAs can act as ‘sponges’, binding to miRNAs, thereby inhibiting their activity and ultimately restoring the expression of miRNA-targeted mRNAs. This regulatory mechanism is referred to as ceRNA [11]. Based on previous research, it has been found that ceRNA networks have a significant impact on cognitive degenerative diseases such as Alzheimer’s, Parkinson’s, autism spectrum disorder, traumatic brain injury as well as ischemic stroke [13–18]. This discovery offers valuable insights into the possible function of ceRNA within POCD.

To examine differences in lncRNA, miRNA, and mRNA expression, we conducted transcriptome sequencing on the hippocampi of young (2 months) and aging (17 months) mice in both normal and laparotomy conditions. Our investigation encompassed GO and KEGG enrichment, which helped identify key biochemical pathways associated with POCD. In addition, we developed the lncRNA-miRNA-mRNA regulatory networks using the ceRNA concept as well as small molecule medications targeting these systems.

The results of our study provide new understandings of the mechanisms behind the start of POCD and possible targets for treatment.

## Methods and materials

### Animal groups

Male C57BL/6 mice, 2 months old (young) and 17 months old (aging), were obtained from the Experimental Animal Center of Guangzhou University of Chinese Medicine. The mice had unrestricted access to food and water and were housed in a controlled environment with a 12-hour light/dark cycle. The following groups were chosen at random from among the young and aging mice: Young Control (YC), Young Surgery (YS), Aging Control (AC), as well as Aging Surgery (AS). Under isoflurane anesthesia, exploratory laparotomies were performed on mice in the surgical groups, while those in control groups were not subjected to any surgical or anesthesia procedures. All animal research used in this work were authorized by the Committee for the Protection and Use of Animals of Sun Yat-sen University (permission number: SYSU-IACUC-2023-000809) as well as the Experimental Animal Ethics Committee of Sun Yat-sen University.

### Anesthesia and surgery

The surgical procedures were carried out on mice under isoflurane anesthesia as previously described [12]. Mice were induced and maintained with 1.5% isoflurane in 1 L/min oxygen. After a 30-minute induction period, a 2 cm incision was made along the abdominal midline, followed by a 2-minute abdominal cavity exploration using a cotton swab. Subsequently, the small intestine was exteriorized and gently rubbed between the thumb and index finger for 3 min. The surgical incision was closed by stitching the muscles and skin using 4–0 surgical sutures, and the entire procedure lasted around 70 min. The mice of the control group did not undergo any surgical procedures or anesthesia.

### Behavioral tests

#### Open field test

The mice underwent an open field test (OFT) on day 7 following surgery to assess their movement patterns and symptoms of anxiety. The OFT was conducted in a blue polyvinyl chloride square open box (50 cm × 50 cm × 50 cm) divided into central and peripheral zones. After

an hour of acclimation to the testing room, each mouse was placed in the center of the box and allowed to move freely. Their actions were recorded employing the ANY-maze open experimental tracking analysis system (Stoelting Co. USA). The total distance traveled and the total duration spent in the center were measured. The area was meticulously cleaned and sprayed with 75% alcohol after each trial to minimize odor contamination.

#### **Y-maze test**

After the OFT, the Y-maze test was employed on mice to determine their spatial recall. The Y-maze consisted of three arms with symmetrical dimensions of 35×5×15 cm, joined at a 120° angle. The mice were allowed to roam the maze freely for 8 min, while a video tracking system (Any-Maze, Stoelting Co., USA) recorded their activities, including the number of entries into each arm. A successful alternation was defined as entries into all three arms in consecutive turns without repeating any arm. The rate of spontaneous alternations was determined by the formula: (Number of successful alternations / (total number of arm entries - 2)) × 100%. The maze arms were sanitized with 75% alcohol to eliminate residual odors following each test.

#### **Novel object recognition test**

A novel object recognition (NOR) test was employed on mice on day 8 following surgery to assess their object recognition memory. The test was conducted in a square open box (50×50×50 cm) made of blue polyvinyl chloride. After a ten-minute acclimatization period within the testing area, the mice were returned to their home cages. The next day, each mouse was reintroduced to the testing area, which contained two identical objects (same shape, size and color) placed in adjacent corners, 10 cm from the walls. One of the familiar objects was replaced with a novel object different in shape, color, and texture, and the mice were again given 5 min to explore. The video tracking system (Any-Maze, Stoelting Co. USA) was employed to document the total time spent by each mouse exploring each object. The fraction of the total exploration time devoted to the new object was used to compute the Recognition Index (RI). All objects were previously tested to avoid biased preference. The box and plastic cubes were wiped with 75% alcohol following each trial to eliminate any residual odors.

#### **Sample preparation**

Twelve hours post-surgery, the mice were anesthetized with isoflurane and then perfused with refrigerated physiological saline solution. The hippocampal tissues were collected for RNA sequencing ( $n=3$  per group) and quantitative real-time polymerase chain reaction

(RT-qPCR) study ( $n=6$  per group). Furthermore, following the behavioral tests, 5 mice from each group were randomly selected for immunofluorescence research, and their brain tissues were collected using the same protocol.

#### **RNA extraction, purification, and RNA sequencing**

A careful extraction of total RNA was performed employing the miRNeasy Mini Kit (217004, Qiagen, GmbH, Germany). Its integrity was then assessed by examining the RIN number using the Agilent Bioanalyzer 2100 (Agilent Technologies, Santa Clara, CA, USA). Eligible total RNA samples were then refined and purified employing the RNAClean XP Kit (A63987, Beckman Coulter, Inc., Brea, CA, USA) in conjunction with the RNase-Free DNase Set (79254, Qiagen, GmbH, Germany). To ensure the pure nature of the extracted RNA, assessments were conducted utilizing the NanoDrop ND-2000 Spectrophotometer (NanoDrop Technologies, Wilmington, DE, USA) and the aforementioned Agilent Bioanalyzer 2100. Additionally, the RNA quality was further validated through standard denaturing agarose gel electrophoresis.

For lncRNA and mRNA, the RiboZero rRNA Removal Kit (Cat#RZG1224, Illumina) was used to eliminate rRNA. Following that, random segments of RNA samples were created by synthesizing cDNA fragments. The purified double-stranded cDNA underwent adaptor ligation using the VAHTS Total RNA-seq (H/M/R) Illumina Library Kit (NR603-02, Vazyme, CHN). The prepared library was quality-controlled utilizing the Qubit dsDNA HS Assay Kit (Q32854, Invitrogen, Carlsbad, CA, United States) along with sequenced employing the Illumina HiSeq X Ten platform upon passing quality checks.

For miRNA, the NEBNext Multiplex Small RNA Library Prep Set for Illumina (Set 2) (E7580S, NEB, United States) was utilized to ligate the 3' and 5' ends of the extracted RNA. Following reverse transcription and PCR, miRNA was purified and quantified using the Qubit dsDNA HS Assay Kit (Q32854, Invitrogen, Carlsbad, CA, United States), followed by single-end sequencing.

#### **Differentially expressed gene data analysis**

After filtering and aligning raw reads, fold changes of lncRNA and mRNA were determined based on FPKM (fragments per kilo-base of exon model per million mapped reads), while TPM (transcripts per million reads) was employed to estimate miRNA fold changes. The R software's edgeR tool was utilized to find genes that varied in expression throughout all samples. *P* values were calculated using Fisher's exact test and adjusted for multiple testing using the Benjamini-Hochberg procedure. The selection criteria for differentially expressed

lncRNAs and miRNAs were  $|\text{Fold Change}| \geq 2$ ,  $P < 0.05$ . To obtain more mRNAs for functional enrichment analysis, the screening criteria were set at  $|\text{Fold Change}| \geq 1.2$ ,  $P < 0.05$ , and count  $> 30$  in all samples [13].

#### Gene annotation and enrichment analysis

GO Biological Process and KEGG analysis were conducted utilizing Metascape (metascape.org), a bioinformatics application available online that can manage several gene lists. The GO serves as a comprehensive database, established by the Gene Ontology Consortium, that categorizes and describes gene and protein functions into three groups: Biological Process, Cellular Component, and Molecular Function. KEGG serves as a database for systematically analyzing gene functions and genomic data.

The analysis workflow is as follows. Step one: Convert the uploaded gene symbols into corresponding Mus musculus Entrez gene IDs. Step two: Use Circos to display overlap between lists and genes overlapping in function or pathway. Step three: Annotate gene functions using GO and KEGG. Step four:  $P$  values are determined by taking the cumulative hypergeometric distribution and setting thresholds of at least three words and an enrichment factor greater than 1.5.  $P < 0.05$  is regarded as significant and is visualized employing the “ggplot2” package within the R software. Step five: Visualize a term of interest using the membership search function.  $P$  values are computed using the cumulative hypergeometric distribution, with  $P < 0.05$  considered statistically significant.

#### CeRNA network construction

The ceRNA regulatory network of mRNA-lncRNA-miRNA centered on miRNAs was constructed based on differential gene expression profiles. We identified the mRNAs targeted by differentially expressed miRNAs by combining the results from miRanda and miR-Tarbase tools, which identify mRNAs based on seed sequence matching and experimental validation strategies, respectively [14, 15]. The targeted lncRNAs were predicted using miRcode [16]. The intersection of the predicted results and the sequencing results was then taken. Cytoscape was used to construct and visualize the ceRNA regulatory network based on the interrelationships among lncRNAs, miRNAs, and mRNAs.

#### Real-time qPCR validation

Using Trizol reagent (Invitrogen), total RNA was isolated from the hippocampal tissues of mice. The NanoDrop 1000 spectrophotometer (Thermo Science) was used to evaluate the RNA quantity and quality. lncRNAs and mRNAs were reverse transcribed using PrimeScrip RT Master Mix (Cat#RR036A, Takara) and measured with

the TB Green PreMix Ex Taq reagent kit (Cat#RR820A, Takara). MiRNAs were then reverse transcribed and measured using the miDETECT A Track miRNA RT-qPCR Starter Kit (Cat#R11068.5, RiboBio). Real-time qPCR was carried out on a Light Cycler 480 real-time PCR system (Roche Applied Science). GAPDH served as the internal reference gene for lncRNAs as well as mRNAs, while U6 was used for miRNA. We used the  $2^{-\Delta\Delta\text{-Ct}}$  technique to determine the relative expression level. Sequence-specific primers for U6 and miRNAs were designed by RiboBio (Guangzhou, China). Table 1 lists the particular primer pairs used in the investigation.

#### Immunohistofluorescence

After perfusion with pre-chilled saline, the brain was quickly removed and fixed in 4% paraformaldehyde at 4 °C. After that, it was immersed in 10%, 20%, and 30% sucrose solutions consecutively for 24 h each. The brain tissue was separated into 15  $\mu\text{m}$  fresh frozen slices, embedded in optimal cutting temperature (OCT) compound, and then immunostained for DCX. The sections were subjected to three PBS washes with 0.3% Triton X-100, an hour-long incubation in blocking solution (3% BSA, 0.3% Triton X-100 in PBS), and an overnight incubation at 4 °C with rabbit anti-DCX diluted 1:600 (4604 S, Cell Signal Technology Inc. Danvers). Following

**Table 1** Primers sequence for RT-qPCR

Gene	Sequences
NONMMUT062908.2	Forward: TGAATTTGATGTGGGCTGGGTCTG Reverse: GGCTCCTCACTCCGTGGTCTC
NONMMUT069618.2	Forward: GGGTCTCTGGCTGTCTAGGGAAG Reverse: TTCAACGAGTCAACTCCGAGAACAC
NONMMUT137220.1	Forward: CCCAGAGGACAACCTTGAGCAGAATC Reverse: CGGCACACCTTCCAAAGAGACAG
NONMMUT029772.2	Forward: ATGACATGATCCAGCAGACCCAAATG Reverse: GCAGATGACGGTAGACCTTGTTTC
Ppap2b	Forward: CAAAGCTACAAGTACGACAAGG Reverse: CTTAATGGTGCTGTCTCGATG
Plxnb3	Forward: AGGATGCGAACCCAAGGAGGAG Reverse: AGGAGGAGGCTGGATGAGTTGAC
Snap91	Forward: TACCACCACTGCCACCACCTC Reverse: GTGCCAAACAGGTCTATGCTAGGAG
Sox10	Forward: CTGAGCTCAGCAAGACACTAG Reverse: GTTGGTACTTGTAGTCCGGATG
Arpp19	Forward: TGAAGAAGCAAAGTTAAAGGCAAGG Reverse: TCACCAGTGACCTCTGTCTTATCC
Fbxl2	Forward: TCTGTGCCTCTCGGGTTGTAG Reverse: ACATTCTCAAGGTCCATCTTCTCC
Nek7	Forward: ACTCAGTTCAGCCACAGAAGG Reverse: GGCACTCCATCCAAGAGACAGG

washing, the sections were treated with goat anti-rabbit secondary antibody (Jackson ImmunoResearch Laboratories Inc. #111-545-144) biotin-labeled for two hours at 4 °C. Cell nuclei were stained with Hoechst 33,342 (1: 10,000, Sigma-Aldrich, #14533) at room temperature for 15 min. Images of the hippocampal DG region were captured from three successive coronal sections using an FV3000 confocal microscope and processed with FV31S-SW Viewer. DCX-positive cells in the hippocampal DG region were manually quantified by researchers blinded to the conditions using ImageJ (1.8.0) software. Each assay was performed in at least three independent experiments, with the mean value of each sample representing the count of DCX-positive cells in the DG region for each animal.

### **Drug prediction**

The Connectivity Map (clue.io) is a comprehensive resource that catalogues numerous gene expression profiles influenced by various drugs. This facilitates the prediction of potential therapeutic agents by comparing these profiles with the gene expression patterns linked to specific diseases. Genes' differential expression between the AC group and the AS group was inputted into the Cmap database to predict potential treatments for POCD.

### **Statistical analysis**

Statistical analyses and graphing were executed using GraphPad Prism 8.0 and the R software. The Student's t-test was applied for calculating *P* values for RT-qPCR outcomes. Behavioral and immunofluorescence data were analyzed using two-way ANOVA. If the assumption of homogeneity of variances was met (assessed via Levene's test), Tukey's post hoc test was used for multiple comparisons following ANOVA. In cases where this assumption was not met, the Games-Howell test was applied. A *P* value of 0.05 or lower was considered statistically significant.

## **Results**

### **Anesthetic surgery induces memory decline in aging mice**

Given the higher prevalence of POCD in elderly individuals, our study included young and aging mice to investigate whether a high incidence of POCD also occurs in our mouse model (Fig. 1A). We conducted three different behavioral tests from day 7 to day 10 post-surgery, including an open field test to assess spontaneous movement as well as symptoms of anxiety (Fig. 1B). The findings demonstrated that aging significantly affected motor activity in aging mice ( $F_{1, 28} = 8.933$ ,  $P < 0.01$ ), but the surgical exposure did not affect motor activity in young or aging mice (Fig. 1C). Additionally, aging, not surgery,

had a noteworthy main effect on the proportion of time spent in the center ( $F_{1, 28} = 5.387$ ,  $P < 0.05$ ) (Fig. 1D). We also assessed hippocampal-dependent memory using Y-maze and NOR tests [22, 23]. Our findings revealed that surgery significantly decreased the percentage of spontaneous alternation in Y-maze ( $F_{1, 28} = 16.94$ ,  $P < 0.001$ ) (Fig. 1E) and recognition index in NOR ( $F_{1, 28} = 6.839$ ,  $P < 0.05$ ) (Fig. 1F) in aging mice but not in young ones, although the interaction between surgery and aging was not statistically significant. Representative heat maps from Y-maze test (Fig. 1G) demonstrate the spontaneous alternation behavior patterns across all experimental groups. Representative heat maps from the NOR test (Fig. 1H) illustrate the spatial distribution of exploration activity, with warmer colors indicating areas of increased exploration time, showing notably reduced novel object exploration in the aging surgery group.

### **Alterations in GO and KEGG pathways due to aging**

According to the fundamental principle of molecular biology, genes are transcribed into mRNA, which is then translated into proteins, enabling biological processes. Given previous findings on the relationship between aging and mouse behavior, we investigated the effects of aging on the hippocampal transcriptome. Through RNA sequencing, we found that aging induced significant changes in gene expression within the hippocampus under both control or surgical conditions (Fig. 2A, B). Compared to young mice, aging mice exhibited a large number of differentially expressed genes under both control and surgical conditions. Specifically, under control conditions, 256 mRNAs were upregulated and 235 were downregulated, while under surgical conditions, 225 mRNAs were upregulated and 177 were downregulated. Although there was little overlap in these differentially expressed genes in these two conditions (Fig. 2C), we identified some common biological processes in our functional enrichment analysis. For example, under control conditions, upregulated genes in aging mice were enriched in pathways related to synapses, dendrites, axons, learning, and memory (Fig. 2D), while under surgical conditions, upregulated genes in aging mice were enriched in pathways related to synapses, dendrites, cognition, learning, and memory. Regarding downregulated genes in aging mice, we found that under control conditions, these genes were enriched in pathways related to NF- $\kappa$ B, TNF signaling, GABAergic synapses, neuronal projection development, and RNA localization (Fig. 2F), while under surgical conditions, downregulated genes in aging mice were enriched in pathways related to neuronal differentiation, cellular projections, axon formation, axon development, and neuronal projection development (Fig. 2G). Notably, downregulated genes under

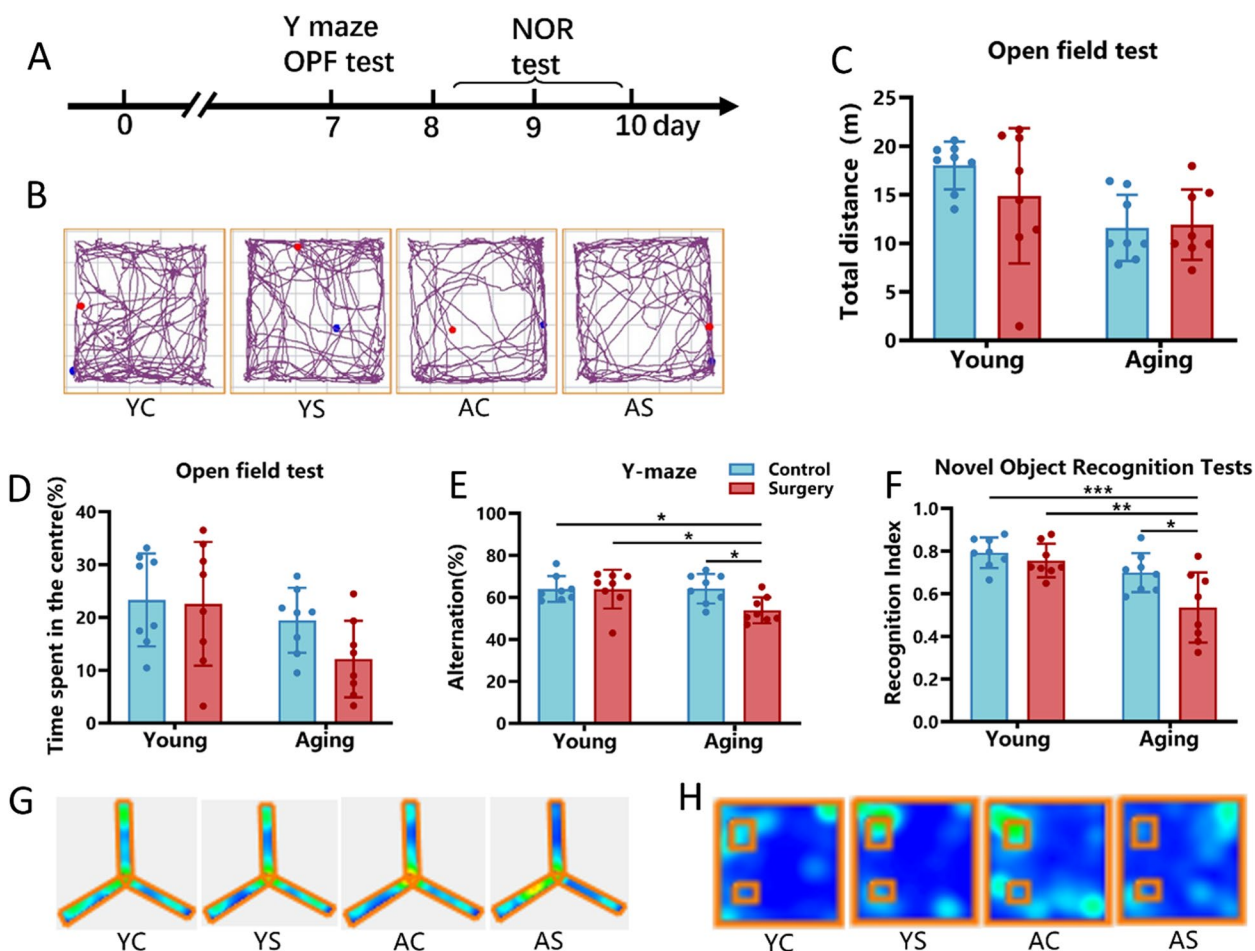


**Fig. 1** Anesthetic surgery induces memory decline in aging mice. **A** Schedule for conducting behavioral studies. **B** Representative tracks from open field test. **C** The total distance covered during open field test. **D** Time spent in the center for open field test. **E** Percentage of spontaneous alternations in Y-maze tests. **F** Recognition index in novel object recognition test. **G** Representative heat maps from Y-maze test. **H** Representative heat maps from Novel Object Recognition test. \* $P < 0.05$ , \*\* $P < 0.01$ , \*\*\* $P < 0.001$  for two-way ANOVA followed by Tukey's post hoc test. Data are presented as means  $\pm$  S.D ( $n = 8$ )

both conditions were enriched in the “neurogenesis” (GO:0022008) as well as the “positive regulation of neurogenesis” (GO:0050769) pathway (Fig. 2J, K).

**Postoperative transcriptional changes in the hippocampus of young and aging mice**

We wondered whether the weaker surgical recovery in aging mice was likely caused by dysregulated gene expression in the hippocampus after behavioral tests revealed post-surgical cognitive impairment within aging mice instead of young ones. Thus, we tested the surgery-induced expression changes of lncRNA, miRNA and mRNA in both young and aging mice. Compared to the control group, the hippocampi of young mice exhibited 744 upregulated and 920 downregulated lncRNAs (Fig. 3A), 13 upregulated and 15 downregulated miRNAs (Fig. 3B), and 136 upregulated and 205 downregulated

mRNAs (Fig. 3C) after surgery. Aging mice post-surgery displayed 952 upregulated and 814 downregulated lncRNAs in the hippocampus (Fig. 3D), 5 upregulated and 6 downregulated miRNAs (Fig. 3E), along with 177 upregulated and 160 downregulated mRNAs (Fig. 3F) compared with the corresponding controls. Young and aging mice showed similar numbers of differentially expressed lncRNAs and miRNAs; however, young mice had much fewer differentially expressed mRNAs than aging mice. Moreover, the fold-changes in the differential expression of these RNAs were significantly higher in the former group (young mice) (Fig. 3G).

**Surgery exacerbated the decrease in neurogenesis observed in aging mice**

Following surgery, young mice exhibited an increase in gene expression linked to brain development, head

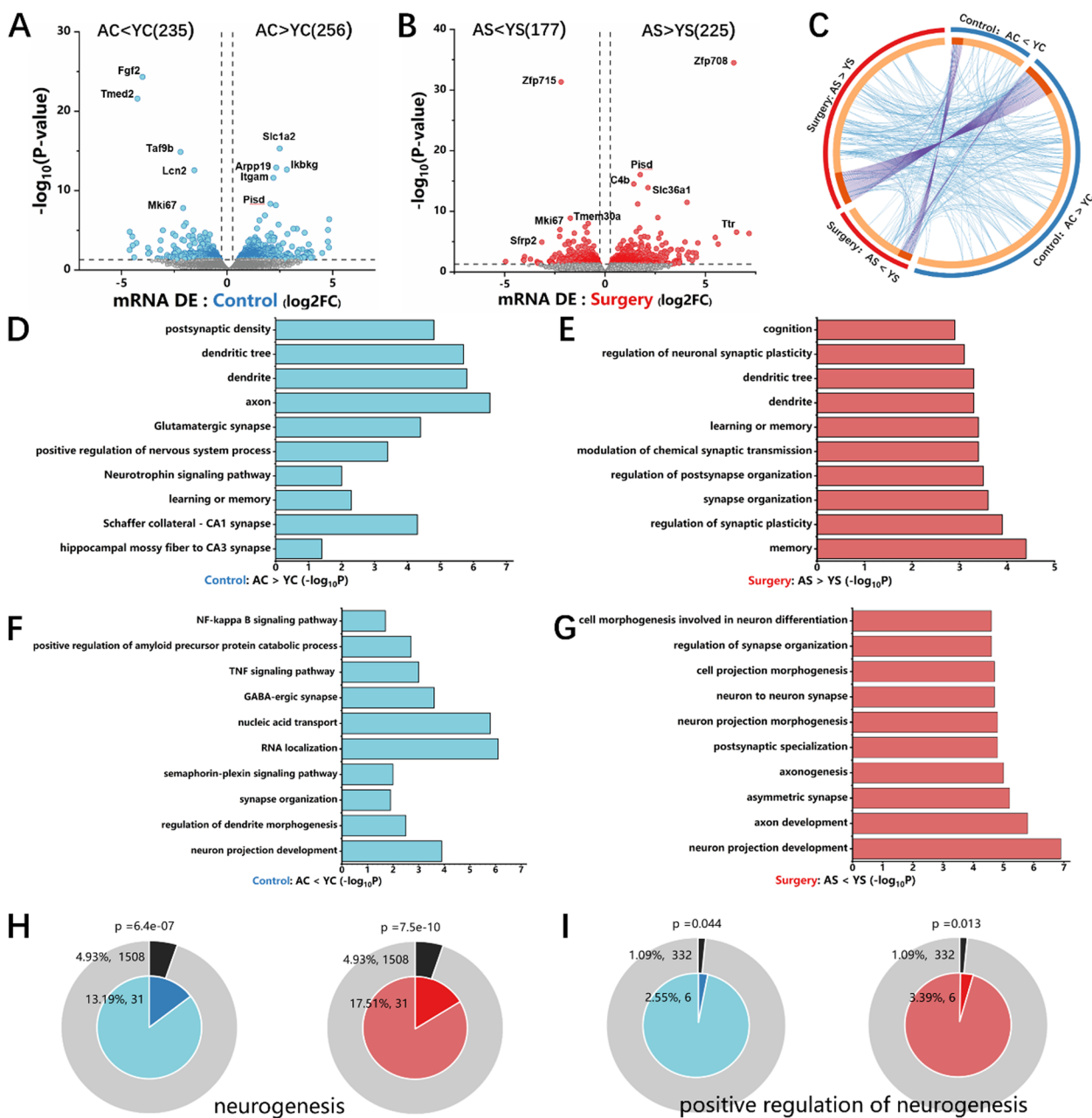


**Fig. 2** Alterations in GO and KEGG pathways due to aging. Blue and red colors represent control and surgical conditions, respectively. **A-B** Volcano plots showing differentially expressed genes in aging mice compared to young mice under control and surgical conditions. Blue (A) and red (B) dots represent significantly differentially expressed genes under control and surgical conditions respectively, while grey dots indicate non-significantly changed genes. The direction and number of expression changes are indicated at the top of each volcano plot. **C** A circular diagram showing the overlap among genes and groups of functions based on four input gene lists. **D, E** Pathways enriched in genes upregulated in aging vs. young mice under control and surgical conditions. **F, G** Pathways enriched in genes downregulated in aging vs. young mice under control and surgical conditions. **H** Enriched GO term 'neurogenesis' (GO:0022008). The black pie represents the proportion of genes related to 'neurogenesis' (GO:0022008) gene ontology term within the genome (gray). The red and blue pies respectively represent the proportions of genes (darker color) related to the GO:0022008 term among the genes that are downregulated in aging mice relative to young mice under control (blue) or surgical conditions (red). *P* values were determined based on the hypergeometric distribution (comparing the proportion of dark-colored slice to the whole colored pie versus the proportion of dark gray slice to the whole gray pie). **I** Enriched GO term 'positive regulation of neurogenesis' (GO:0050769). Color scheme and *P* value calculation are consistent with panel H

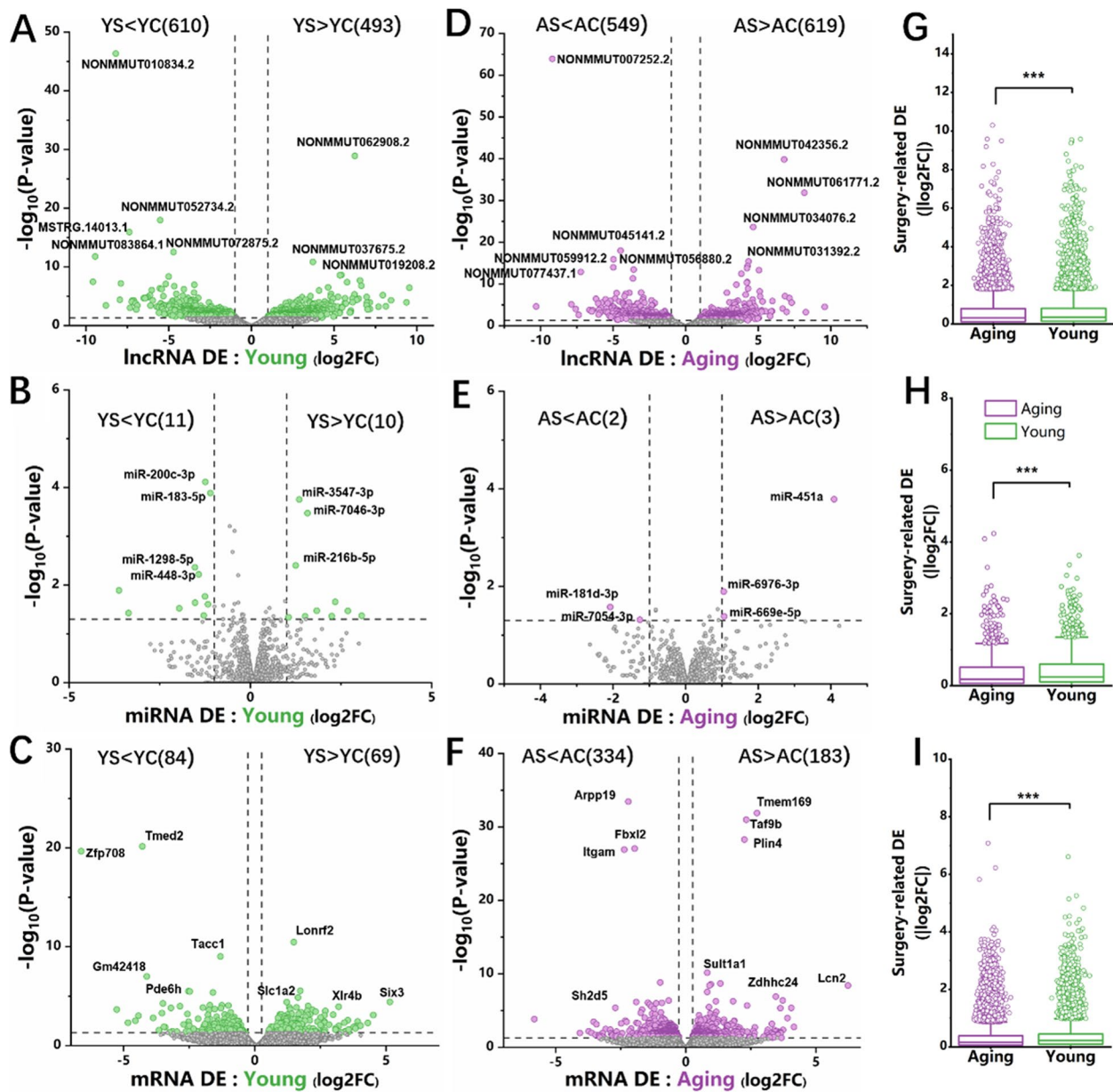


**Fig. 3** Transcriptional changes in the hippocampus of young and aging mice post-surgery. **A-C** Volcano plots of differentially expressed lncRNA, miRNA, mRNA between young surgical and control groups. **D-F** Volcano plots of differentially expressed lncRNA, miRNA, mRNA between aging surgical and control groups. **G-I** Differential magnitude of surgery-related changes in lncRNA, miRNA, mRNA between young and aging mice (y-axis =  $|\log_2 \text{fold-change}|$ ). Whiskers denote the inner fences, circles represent outliers. The *P* value was calculated with the Wilcoxon matched-pairs signed rank test, \*\*\**P* < 0.001

development, neurotransmission, axon guidance and axonogenesis, according to GO enrichment analysis (Fig. 4A). Meanwhile, aging mice showed an increase in gene expression related to NF-κB, apoptotic cell clearance, Rac protein signal transduction and PI3K-Akt signaling pathway (Fig. 4B). The downregulated mRNAs in post-surgical young mice were enriched in cellular respiration, ATP biosynthetic process, astrocyte projection

and ATP metabolic process (Fig. 4C). The downregulated mRNAs in the aging post-surgical mice were primarily abundant in dendritic spine, postsynaptic density, neuron spine axon and dendrite (Fig. 4D). Notably, genes downregulated in both young and aging mice following surgery were significantly enriched in the process of ‘neurogenesis’ (GO:0022008). However, aging mice showed a greater downregulation of neurogenesis-related genes, such as

Ppab2b, Plxnb3, Snap91, and Sox10 (Fig. 4E-I). To further confirm our findings, we conducted DCX immunofluorescent staining and noted that there was a decline in the number of newly generated neurons under both control and surgery conditions during aging. However, upon analyzing the effect of surgery on neurogenesis in mice of different ages, it was clear that the number of freshly produced neurons following surgery was significantly reduced only in aging mice, while such a decline was non-significant in young mice. A two-way analysis of variance revealed a substantial main effect on both age ( $F_{1, 16} = 177.5$ ,  $P < 0.001$ ) and surgery ( $F_{1, 16} = 10.21$ ,  $P < 0.01$ ), but not for the interaction between age and surgery ( $F_{1, 16} = 4.025$ ,  $P = 0.062$ ) (Fig. 4J, K).

#### Identification of neurogenesis-associated lncRNAs in aging mice

The ceRNA mechanism, through which lncRNAs can competitively bind to miRNAs to regulate gene expression, has been demonstrated to participate in numerous physiological processes. To comprehend the connection between differential gene expression and cognitive dysfunction in post-surgical aging mice, a ceRNA network has been developed using the surgery-induced differentially expressed lncRNAs, miRNAs, and mRNAs through seed sequence matching methods and linear regression models (Fig. 5A). Thus, based on the known ceRNA networks, we may deduce the biological functions of lncRNAs in the control of gene expression. Four lncRNAs - NONMMUT062908.2, NONMMUT069618.2, NONMMUT137220.1, and NONMMUT029772.2 (Fig. 5B-E), which were associated with neurogenesis pathways, were found in our ceRNA networks and their expression patterns were confirmed via RT-qPCR (Fig. 5F-I). We randomly selected two miRNAs and three mRNAs that were strongly linked to the aforementioned lncRNAs for RT-qPCR validation to further validate those lncRNA-associated ceRNA networks. The findings demonstrated that following surgery, the hippocampi of aging mice exhibited substantially higher levels of miR-6976-3p and miR-6985-5p in comparison to the control group,

while mRNAs such as Arpp19, Fbxl2 and Nek7 were significantly downregulated (Fig. 5J-N). The precision and dependability of the ceRNA networks were improved by our RT-qPCR outcomes, which also confirmed the RNA sequencing findings.

#### Prediction of potential therapeutic drugs

The Cmap (clue.io) database contains differential gene expression profiles following treatment with thousands of drugs in various cell types. Lists of differentially expressed mRNAs from the aging surgical group compared to the aging control group, were uploaded to this database to predict potential therapeutic small molecule drugs. The analysis calculated.

the weighted enrichment score (WTCS) between the query and each of the over 1 million level 5 reference signatures. WTCS values are then normalized by dividing by the signed mean within each subset of reference signatures, grouped by cell line and perturbagen type, resulting in normalized connectivity scores (Normalized CS). When the NCS for a compound is negative, it suggests that the compound may attenuate or reverse the differential gene expression. The term 'target gene' in this context refers to the number of genes that intersect each drug's gene targets and the list of genes with differential expression. The top 10 ranked drugs are shown in the table, including ziprasidone, thioridazine, and oxcarbazepine, which reversed the most genes and had relatively large negative scores. This suggests that these three medications could potentially treat POCD. Their molecular diagrams are shown in Table 2; Fig. 6.

#### Discussion

Previous studies have suggested that elderly individuals are more susceptible to POCD [17, 18], potentially due to the decline of various neuro-related mechanisms in the aging hippocampus [19]. While prior research has established this susceptibility, our study makes several novel contributions to the field: (1) We provide the first comprehensive comparison of hippocampal gene expression patterns between young and aging mice under both

(See figure on next page.)

**Fig. 4** Surgery exacerbated the decrease in neurogenesis in aging mice. **A, B** Pathways enriched in genes upregulated in young and aging mice post-surgery relative to their age-matched controls. **C, D** Pathways enriched in genes downregulated in young and aging mice post-surgery relative to their age-matched controls. **E** In the gene enrichment study, the grey pie represents the proportion of 'neurogenesis' (GO:0022008) ontology term-related genes in the genome, and the black area represents the rest of the genome. The green and purple pies represent the proportion of genes (darker color) related to the GO:0022008 term among the genes that are downregulated in young (green) and aging (purple) mice post-surgery compared to their age-matched controls. **F-I** qPCR verification of representative genes enriched in 'neurogenesis' (GO:0022008) GO term among differentially expressed genes in aging mice post-surgery relative to age-matched controls ( $n = 6$ , per group). **J** Confocal images of DCX antibody immunofluorescence staining (Blue, Hoechst 33342; Green, DCX;  $n = 5$ , per group). Top left, top right, bottom left, and bottom right are representative images from YC, YS, AC, and AS mouse groups, respectively. **K** Effects of aging and surgery on DCX positive cell density (relative to young control). \* $P < 0.05$ , \*\* $P < 0.01$ , \*\*\* $P < 0.001$  for two-way ANOVA followed by Games-Howell test. Data are presented as means  $\pm$  S.D. ( $n = 5$ )

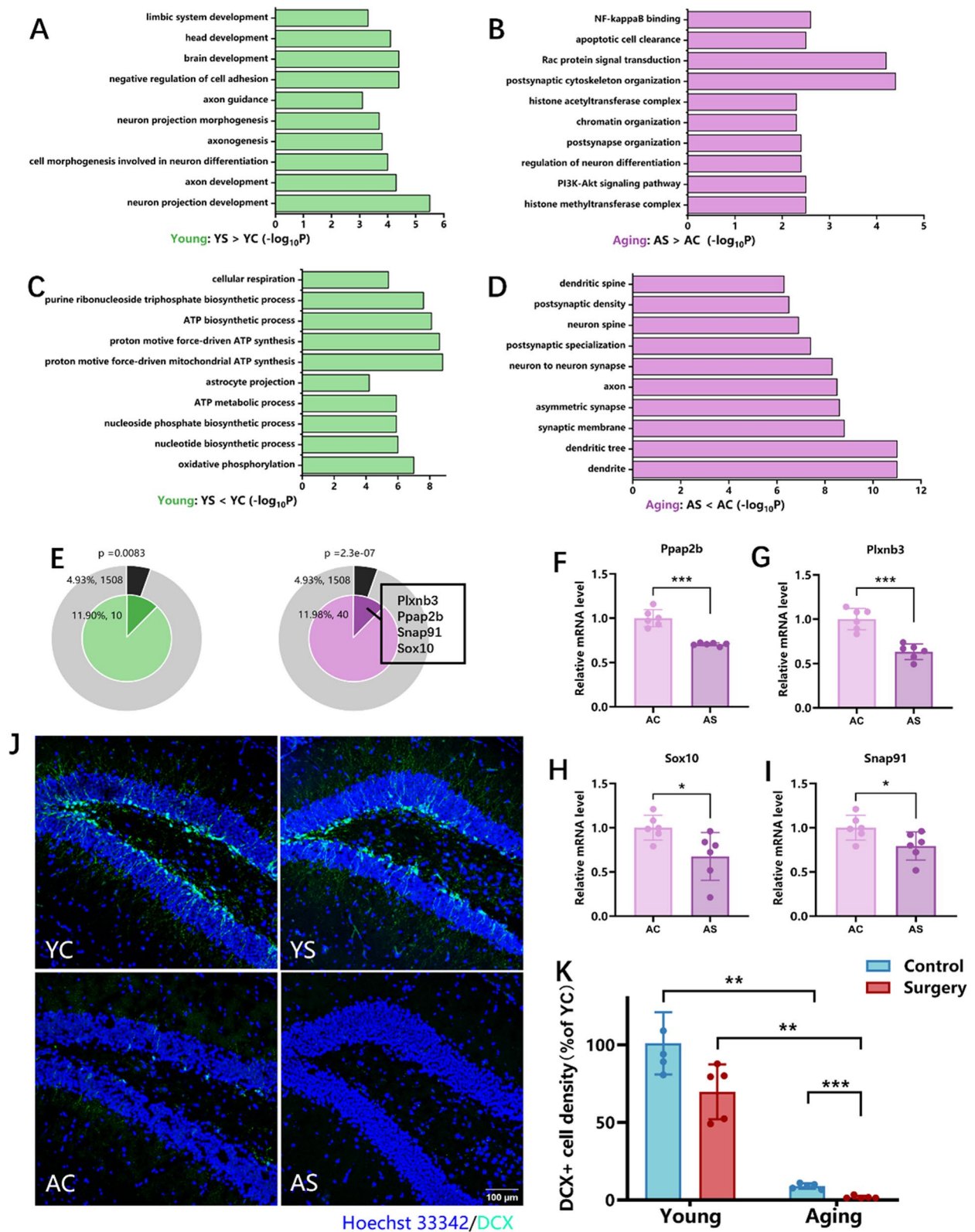


Fig. 4 (See legend on previous page.)

control and surgical conditions, (2) We identify specific molecular signatures that distinguish age-dependent POCD vulnerability, and (3) We reveal previously unreported ceRNA networks that may regulate post-surgical neurogenesis.

Unlike our previous study, which used fear conditioning and Barnes maze to assess learning and recall function in post-surgical mice, we used Y-maze as well as NOR test within the current research. Similarly, our behavioral tests showed that hippocampal-related memory impairment was generated by anesthesia and surgery in aging mice, but not in young ones, which is consistent with our previous study and other studies [20, 21], and lay a solid foundation for POCD research based on our mouse model.

To gain deeper insights into the etiology of postoperative cognitive dysfunction (POCD), we first explored the impact of aging on hippocampal gene expression under control and surgical conditions. Under control conditions, aging mice exhibited upregulation of several genes related to axonal and dendritic structures, synapses in the CA1 and CA3 pathways, glutamatergic synapses, and neurotrophic factor signaling pathways when compared to young mice. Notably, elevated levels of Apod have been linked to cognitive decline in Alzheimer's disease patients [22]; overexpression of Atf4 inhibits long-term synaptic changes and memory formation, leading to impaired memory [23]; upregulation of C4b may cause excessive synaptic pruning, resulting in cognitive dysfunction [24]. Conversely, genes such as CaMKII $\alpha$  and Sdc3 play crucial roles in synaptic function and neuronal development. CaMKII $\alpha$  is essential for the induction of long-term potentiation (LTP) and enhances synaptic transmission efficacy [25], while deficiency in Sdc3 can lead to hippocampus-dependent memory impairments [26]. Simultaneously, aging mice showed downregulation of genes associated with neural projection development, dendrite morphogenesis, synapse organization, GABAergic synapses, and the TNF and NF- $\kappa$ B signaling pathways. This downregulation may contribute to synaptic dysfunction and increased neuroinflammation. For instance, decreased expression of Gabra2 may lead to neuronal hyperexcitability and subsequent cognitive

deficits [27]; downregulation of Gfra1, which interacts with the neurotrophic factor GDNF to regulate integration of newborn neurons and synaptic plasticity, may affect cognitive function [28]; overexpression of Vcam1 during neuroinflammation is associated with cognitive decline [29].

Under surgical conditions, aging mice, in comparison to young mice, exhibited upregulation of genes associated with the regulation of synaptic plasticity and cognition. Among these upregulated genes, Apoe is considered a marker of Alzheimer's disease, with increased levels closely linked to cognitive impairment [30, 31]; S100b, a calcium-binding protein secreted by astrocytes, is involved in neuronal survival and neuroplasticity, but elevated levels are associated with neuroinflammation and neurodegenerative diseases [32]; Gfap, an astrocyte marker, may be overactivated in cognitive impairment in mice [33]; Tshz3 plays a role in neural development, and its haploinsufficiency is associated with autism spectrum disorders and cognitive dysfunction [34]. Conversely, aging mice significantly downregulated genes crucial for cognitive processes, including those related to axon development, synapse organization, and neuronal projection morphogenesis. Downregulated genes such as Chl1, a neural cell adhesion molecule whose deficiency can lead to shortened working memory duration [35]; Dcx, involved in neuronal migration and adult neurogenesis, where its reduction may be associated with cognitive deficits [36]; and MyoVb, which is involved in vesicle transport and receptor recycling, affecting AMPA receptor recycling and thereby influencing synaptic plasticity and memory [37].

Subsequently, we investigated the differentially expressed mRNAs in the hippocampus of young and aging mice under surgical conditions. In young mice, compared to their age-matched controls, surgery induced upregulation of mRNAs primarily enriched in pathways related to neural projection development, axon development, cell morphogenesis involved in neuron differentiation, and axonogenesis. Among these upregulated genes, Nfix is essential for hippocampal development and function; its deficiency leads to abnormal hippocampal structure and impaired learning and memory [38]. Loss of

(See figure on next page.)

**Fig. 5** Identification of neurogenesis-associated lncRNAs in aging mice. **A** Differential expression of lncRNAs, miRNAs, and mRNAs between aging mice within the surgery as well as the control group, with a constructed ceRNA network based on their interactions. **B-E** Representative lncRNAs whose downstream mRNAs are enriched in the 'neurogenesis' (GO:0022008) GO term. The gray pies illustrate the proportion of 'neurogenesis' (GO:0022008) GO term-related genes (dark color) in the genome. The orange, cyan, purple, and pink pies represent the proportions of mRNAs (darker color), downstream of four different lncRNAs and enriched in GO:0022008 term among all downstream mRNAs of the respective lncRNA. **F-I** Expression of NONMMUT062908.2, NONMMUT069618.2, NONMMUT137220.1, and NONMMUT029772.2 was verified within the aging control as well as the aging surgery group using RT-qPCR ( $n=6$ ). **J-N** The validation findings of miR-6976-3p, miR-6985-5p, Arpp19, Fbxl2 and Nek7 by RT-qPCR. \* $P < 0.05$  contrasted with the control group, \*\* $P < 0.01$  contrasted with the control group, \*\*\* $P < 0.001$  compared to the control group

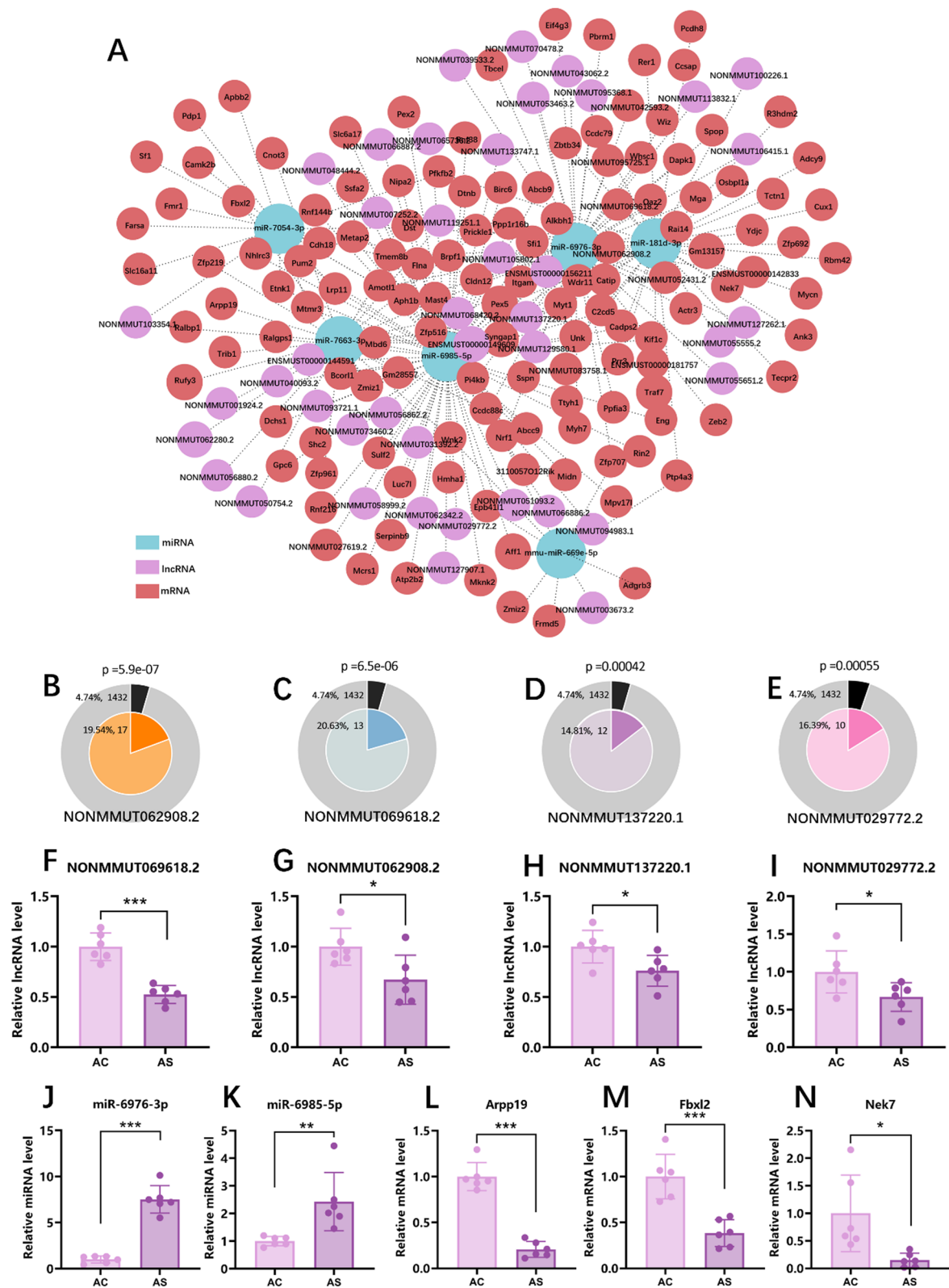


**Fig. 5** (See legend on previous page.)

**Table 2** The top 10 small molecular drugs with high negative correlations with POCD

Rank	Cmap name	Target gene	Q value	Normalized CS
1	ziprasidone	26	4.4412E-16	-1.4322
2	thioridazine	16	4.4412E-16	-1.4539
3	oxcarbazepine	13	4.4412E-16	-1.563
4	sotrastaurin	6	4.4412E-16	-1.513
5	tolazoline	6	4.4412E-16	-1.4596
6	aniracetam	6	4.4412E-16	-1.4575
7	pasireotide	5	4.4412E-16	-1.6102
8	vanoxerine	3	4.4412E-16	-1.4583
9	tanespimycin	2	4.4412E-16	-1.4504
10	chaetocin	1	4.4412E-16	-1.4306

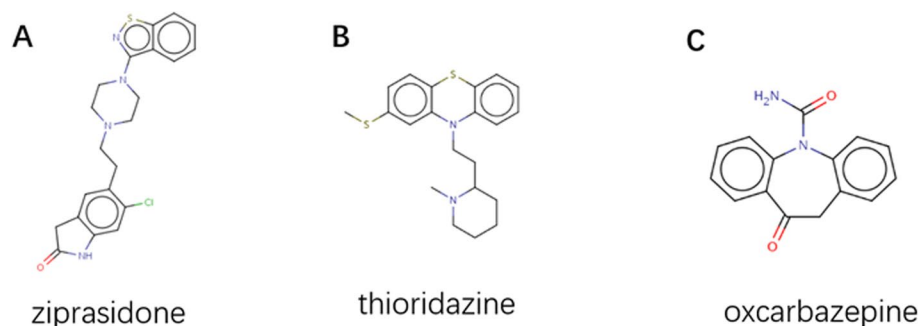
Foxp1 blocks synaptic and network hallmarks of memory formation [39], while upregulation of DRR1 enhances hippocampus-dependent memory [40]. Additionally, Apod expression was increased in the hippocampus of young mice post-surgery. Conversely, downregulated genes in young mice after surgery were enriched in mitochondrial pathways and astrocyte projections. For example, ATP6 and ATP8 are subunits of mitochondrial ATP synthase, and ND2 and ND4L are subunits of NADH dehydrogenase, all involved in mitochondrial energy metabolism. Mutations in these genes can lead to mitochondrial dysfunction, which is associated with various neurodegenerative diseases [41–46]. Furthermore, deficiency of Aqp4 impairs synaptic plasticity in the lateral amygdala and associative fear memory [47].

In aging mice, surgery led to upregulation of genes mainly enriched in postsynaptic cytoskeleton organization, Rac protein signal transduction, apoptotic cell clearance, NF- $\kappa$ B binding, and PI3K-Akt pathways, compared to their age-matched controls. Among these upregulated genes, inhibition of Hdac9 increases CaM acetylation in AD mice, improving hippocampus-dependent memory [48]; overexpression or increased activity of

Eif4e is associated with autism-like behaviors [49]; over-activation of Fgfr3 contributes to memory impairment in mouse models of Crouzon syndrome [50]; deletion of Rac1 impairs synaptic plasticity in the hippocampus, leading to spatial learning deficits [51]. Simultaneously, the downregulated genes in aging mice post-surgery were enriched in pathways related to dendrites, synaptic membranes, asymmetric synapses, axons, and neuronal synapses. Among these downregulated genes, Arc is an immediate early gene critical for regulating synaptic plasticity, learning, and memory; its deficiency leads to long-term memory impairment [52]. Bcan participates in synaptic stabilization and plasticity, exhibiting region-specific upregulation during new memory formation [53]. Cryab can reduce the expression of astrocyte neurotoxic response genes after central nervous system injury [54]; Mag is important for myelin sheath stability and neuron-glia interactions, and myelin damage can lead to cognitive deficits [55].

Notably, the expression of genes associated with neurogenesis is downregulated under various conditions. A substantial body of evidence supports that neurogenesis itself contributes to the formation of hippocampus-dependent memories [56, 57]. Reports indicate that neurogenesis decreases sharply in aged rats compared to adult rats [58], which aligns with our DCX immunofluorescence experimental results. Furthermore, when compared to age-matched control groups, the number of neurogenesis in aging mice decreased significantly post-surgery, whereas this reduction was less pronounced in young mice.

The degree of memory impairment in aged rats has been quantitatively linked to hippocampal neurogenesis [59], and we observed a similar association in our DCX immunofluorescence experiments and behavioral studies. For instance, the aging surgical group showed a significant decrease in neurogenesis in the hippocampal dentate gyrus compared to the aging control group, young control

**Fig. 6** The composition of possible medicinal substances. **A** The chemical structure of ziprasidone. **B** The chemical structure of thioridazine. **C** The chemical structure of oxcarbazepine

group, and young surgical group. Correspondingly, the behavioral performance of mice in the aging surgical group was significantly worse than that of the other three groups. Interestingly, although the aging control mice exhibited a significant reduction in neurogenesis compared to the young control mice, there was no significant difference in behavioral performance between the two groups during behavioral tests, except for a trend toward decreased performance in novel object recognition. This phenomenon may be related to the presence of a certain number of newborn neurons in the hippocampal dentate gyrus of the aging control mice. It has suggested that there may be a critical threshold of neurogenesis below which significant behavioral effects become apparent [60]. Additionally, this observation may be influenced by the lower spatially separation of stimuli of behavioral or the small sample size in our study. The previous research indicated that spatial memory is impaired in adult mice with ablated hippocampal neurogenesis when stimuli are less spatially separated, but not when stimuli are more widely separated. In subsequent, more in-depth mechanistic studies, we plan to increase the sample size and employ more challenging behavioral tests to explore this issue.

These results suggest that numerous differentially expressed genes appear in the hippocampus of aging mice as a compensatory response to counteract inflammation and cognitive impairment induced by aging. Under surgical conditions, although this compensatory response persists, it becomes insufficient to mitigate the additional damage, leading to the development of POCD in mice. These findings advance our understanding of age-dependent POCD susceptibility.

Additionally, our study makes a novel contribution by elucidating the complex interaction between surgery and neurogenesis through comprehensive ceRNA network analysis. Specifically, we found that NONMMUT062908.2, NONMMUT069618.2, NONMMUT137220.1, and NONMMUT029772.2 may function as molecular sponges for miR-6976-3p and miR-6985-5p, reducing their availability to bind with neurogenesis-related mRNAs. Under normal conditions, the competitive binding among these RNAs forms a dynamic regulatory network that maintains sufficient neurogenesis. In aging mice post-surgery, dysregulation of this network may lead to impaired proliferation and differentiation of neural progenitor cells and reduced numbers of newborn neurons, ultimately resulting in POCD.

Finally, according to our investigation of differential gene expression, we predicted that ziprasidone, thioridazine, and oxcarbazepine could serve as potential therapeutic drugs for POCD. Ziprasidone is an atypical antipsychotic medication used in the treatment of acute agitation [61]. Oxcarbazepine, unlike other drugs in its class, is an antiepileptic drug that does not have adverse

side effects related to cognitive and psychomotor disorders. It may even enhance performance on tasks requiring concentrated attention [62]. But no published research has explored this potential, and more in-depth investigation is needed to determine the viability and mechanisms of action, which could lead to new research directions.

It is important to recognize the limitations of the current investigation. First, since anesthesia and surgery are interwoven in a clinical context, we did not establish a distinct anesthesia group. Second, the only time point in our sequencing was 12 h after surgery, which is a few days prior to the DCX immunofluorescence tests. Hence, it is difficult to ascertain whether any new gene expression dysregulations occurred during this interval, contributing to the decline in neurogenesis. Furthermore, to avoid potential confounding effects of estrous cycles on female mouse cognition, the study was restricted to male mice; therefore, further research using female mice is necessary to determine whether POCD involves sex-specific mechanisms. Lastly, the prediction of the lncRNA-miRNA-mRNA axis is primarily based on bioinformatics analysis. Further experimental verification is needed to determine whether the specific lncRNAs selected are essential to POCD.

## Conclusion

In summary, this work aims to explore the processes that may contribute to elderly patients' higher susceptibility to POCD. It is the first study to combine the impacts of aging on the hippocampus transcriptome in a POCD mouse model. Through functional enrichment analysis of differentially expressed genes under various conditions, we identified that both aging and surgery lead to a dramatic decrease in neurogenesis, which could underlie the heightened susceptibility to POCD in aging mice. Additionally, our bioinformatic analysis identified putative critical lncRNAs that could be implicated in the pathophysiology of POCD. These findings offer therapeutic targets for prospective novel small molecule medicines and future approaches to treating POCD.

## Supplementary Information

The online version contains supplementary material available at <https://doi.org/10.1186/s12871-025-02928-z>.

- Supplementary Material 1.
- Supplementary Material 2.
- Supplementary Material 3.
- Supplementary Material 4.
- Supplementary Material 5.
- Supplementary Material 6.
- Supplementary Material 7.
- Supplementary Material 8.

## Acknowledgements

We thank Professor Yi Zou for providing the experimental facilities. We also thank Professor Phei-Er Saw for her helpful advice regarding experimental design and data analysis.

## Authors' contributions

Conceptualization, LC and CZF; Methodology, LC, CZF, JRL, XQZ, XL, YH, and SQC; Data Curation, JRL, XQZ, XL, YHL; Writing – Original Draft, JRL; Writing – Review & Editing, LC, and CZF; Visualization, JRL, XQZ, XL, YHL; Supervision, LC; Funding Acquisition, CZF and LC. All authors reviewed the manuscript.

## Funding

This work was supported by grants from the Guangdong Science and Technology Department (2022A1515012396) and the Zhejiang Provincial Natural Science Foundation of China and the Zhejiang Provincial Program (LY22H090011).

## Data availability

The RNA-seq data generated in this study have been deposited in the NCBI Sequence Read Archive (SRA) database under the accession number SRP323354. These data will be made publicly available upon acceptance of the manuscript for publication.

## Declarations

### Ethics approval and consent to participate

All animal research used in this work were authorized by the Committee for the Protection and Use of Animals of Sun Yat-sen University (permission number: SYSU-IACUC-2023-000809) as well as the Experimental Animal Ethics Committee of Sun Yat-sen University.

### Consent for publication

Not applicable.

### Competing interests

The authors declare no competing interests.

### Author details

<sup>1</sup>Department of Anesthesiology, Sun Yat-sen Memorial Hospital, Sun Yat-sen University, Guangzhou, China. <sup>2</sup>The Key Laboratory of Virology of Guangzhou, Jinan University, Guangzhou, China. <sup>3</sup>School of Basic Medical Sciences and Forensic Medicine, Hangzhou Medical College, Hangzhou, China.

Received: 4 October 2024 Accepted: 24 January 2025

Published online: 06 February 2025

## References

- Newman S, et al. Postoperative cognitive dysfunction after noncardiac surgery: a systematic review. *Anesthesiology*. 2007;106(3):572–90.
- Yang X, et al. Identification of individuals at risk for postoperative cognitive dysfunction (POCD). *Ther Adv Neurol Disord*. 2022;15:17562864221114356.
- Evered LA, et al. Prevalence of dementia 7.5 years after coronary artery bypass graft surgery. *Anesthesiology*. 2016;125(1):62–71.
- Rundshagen I. Postoperative cognitive dysfunction. *Dtsch Arztl Int*. 2014;111(8):119–25.
- Kotekar N, Shenkar A, Nagaraj R. Postoperative cognitive dysfunction - current preventive strategies. *Clin Interv Aging*. 2018;13:2267–73.
- Li Z, et al. Neuroinflammation as the underlying mechanism of postoperative cognitive dysfunction and therapeutic strategies. *Front Cell Neurosci*. 2022;16:843069.
- Zhang J, et al. Graphene oxide improves postoperative cognitive dysfunction by maximally alleviating amyloid beta burden in mice. *Theranostics*. 2020;10(26):11908–20.
- Wan Y, et al. Cognitive decline following major surgery is associated with gliosis, beta-amyloid accumulation, and tau phosphorylation in old mice. *Crit Care Med*. 2010;38(11):2190–8.
- Anderson DM, et al. A micropeptide encoded by a putative long noncoding RNA regulates muscle performance. *Cell*. 2015;160(4):595–606.
- Tiwari A, Mukherjee B, Dixit M. MicroRNA Key to Angiogenesis Regulation: MiRNA Biology and Therapy. *Curr Cancer Drug Targets*. 2018;18(3):266–77.
- Tay Y, Rinn J, Pandolfi PP. The multilayered complexity of ceRNA crosstalk and competition. *Nature*. 2014;505(7483):344–52.
- Zhang MX, et al. Characterization of circRNA-Associated-ceRNA Networks involved in the Pathogenesis of Postoperative Cognitive Dysfunction in Aging mice. *Front Aging Neurosci*. 2022;14:727805.
- Lotan A, et al. Differential effects of chronic stress in young-adult and old female mice: cognitive-behavioral manifestations and neurobiological correlates. *Mol Psychiatry*. 2018;23(6):1432–45.
- Betel D, et al. The microRNA.org resource: targets and expression. *Nucleic Acids Res*. 2008;36(Database issue):D149–53.
- Hsu SD, et al. miRTarBase: a database curates experimentally validated microRNA-target interactions. *Nucleic Acids Res*. 2011;39(Database issue):D163–9.
- Jeggari A, Marks DS, Larsson E. miRcode: a map of putative microRNA target sites in the long non-coding transcriptome. *Bioinformatics*. 2012;28(15):2062–3.
- Monk TG, et al. Predictors of cognitive dysfunction after major noncardiac surgery. *Anesthesiology*. 2008;108(1):18–30.
- Luo A, et al. Postoperative cognitive dysfunction in the aged: the collision of neuroinflammation with perioperative neuroinflammation. *Inflammopharmacology*. 2019;27(1):27–37.
- Burke SN, Barnes CA. Neural plasticity in the ageing brain. *Nat Rev Neurosci*. 2006;7(1):30–40.
- Barrientos RM, et al. Intracisternal interleukin-1 receptor antagonist prevents postoperative cognitive decline and neuroinflammatory response in aged rats. *J Neurosci*. 2012;32(42):14641–8.
- Culley DJ, et al. The memory effects of general anesthesia persist for weeks in young and aged rats. *Anesth Analg*. 2003;96(4):1004–9.
- Thomas EA, et al. Apolipoprotein D levels are elevated in prefrontal cortex of subjects with Alzheimer's disease: no relation to apolipoprotein E expression or genotype. *Biol Psychiatry*. 2003;54(2):136–41.
- Chen A, et al. Inducible enhancement of memory storage and synaptic plasticity in transgenic mice expressing an inhibitor of ATF4 (CREB-2) and C/EBP proteins. *Neuron*. 2003;39(4):655–69.
- Aw E, Zhang Y, Carroll M. Microglial responses to peripheral type 1 interferon. *J Neuroinflammation*. 2020;17(1):340.
- Lisman J, Schulman H, Cline H. The molecular basis of CaMKII function in synaptic and behavioural memory. *Nat Rev Neurosci*. 2002;3(3):175–90.
- Kaksonen M, et al. Syndecan-3-deficient mice exhibit enhanced LTP and impaired hippocampus-dependent memory. *Mol Cell Neurosci*. 2002;21(1):158–72.
- Dixon CI, et al. Cocaine effects on mouse incentive-learning and human addiction are linked to alpha2 subunit-containing GABAA receptors. *Proc Natl Acad Sci U S A*. 2010;107(5):2289–94.
- Bonafina A, et al. GDNF and GFRa1 are required for proper integration of adult-born hippocampal neurons. *Cell Rep*. 2019;29(13):4308–e43194.
- Yousef H, et al. Aged blood impairs hippocampal neural precursor activity and activates microglia via brain endothelial cell VCAM1. *Nat Med*. 2019;25(6):988–1000.
- Small GW, et al. Memory self-appraisal in middle-aged and older adults with the apolipoprotein E-4 allele. *Am J Psychiatry*. 1999;156(7):1035–8.
- Raulin AC, et al. ApoE in Alzheimer's disease: pathophysiology and therapeutic strategies. *Mol Neurodegener*. 2022;17(1):72.
- Donato R, et al. Functions of S100 proteins. *Curr Mol Med*. 2013;13(1):24–57.
- Wang G, et al. TLI1A promotes the postoperative cognitive dysfunction in mice through NLRP3-mediated A1 differentiation of astrocytes. *CNS Neurosci Ther*. 2023;29(11):3588–97.
- Roubertoux PL, et al. Construct Validity and Cross Validity of a test battery modeling autism spectrum disorder (ASD) in mice. *Behav Genet*. 2020;50(1):26–40.
- Kolata S, et al. Impaired working memory duration but normal learning abilities found in mice that are conditionally deficient in the close homolog of L1. *J Neurosci*. 2008;28(50):13505–10.
- Lee W, et al. Heat stress-induced memory impairment is associated with neuroinflammation in mice. *J Neuroinflammation*. 2015;12:102.

37. Wang Z, et al. Myosin vb mobilizes recycling endosomes and AMPA receptors for postsynaptic plasticity. *Cell*. 2008;135(3):535–48.
38. Heng YH, et al. NFIX regulates neural progenitor cell differentiation during hippocampal morphogenesis. *Cereb Cortex*. 2014;24(1):261–79.
39. Garcia-Oscos F et al. Autism-linked gene FoxP1 selectively regulates the cultural transmission of learned vocalizations. *Sci Adv*. 2021;7(6).
40. Schmidt MV, et al. Tumor suppressor down-regulated in renal cell carcinoma 1 (DRR1) is a stress-induced actin bundling factor that modulates synaptic efficacy and cognition. *Proc Natl Acad Sci U S A*. 2011;108(41):17213–8.
41. Stendel C, et al. Delineating MT-ATP6-associated disease: from isolated neuropathy to early onset neurodegeneration. *Neurol Genet*. 2020;6(1):e393.
42. De Michele G, et al. Reversible Valproate-Induced Subacute Encephalopathy Associated with a MT-ATP8 variant in the mitochondrial genome. *Front Neurol*. 2018;9:728.
43. Dagar S, et al. Ribosome profiling and Mass Spectrometry reveal widespread mitochondrial translation defects in a Striatal Cell Model of Huntington Disease. *Mol Cell Proteom*. 2024;23(4):100746.
44. Al-Kafaji G, et al. Next-generation sequencing of the whole mitochondrial genome identifies functionally deleterious mutations in patients with multiple sclerosis. *PLoS ONE*. 2022;17(2):e0263606.
45. Wang W, et al. Mitochondria dysfunction in the pathogenesis of Alzheimer's disease: recent advances. *Mol Neurodegener*. 2020;15(1):30.
46. Yan W, et al. Testosterone ameliorates age-related brain mitochondrial dysfunction. *Aging*. 2021;13(12):16229–47.
47. Li YK, et al. Aquaporin-4 deficiency impairs synaptic plasticity and associative fear memory in the lateral amygdala: involvement of downregulation of glutamate transporter-1 expression. *Neuropsychopharmacology*. 2012;37(8):1867–78.
48. Zhang HL, et al. HDAC9-mediated calmodulin deacetylation induces memory impairment in Alzheimer's disease. *CNS Neurosci Ther*. 2024;30(2):e14573.
49. Gkogkas CG, et al. Autism-related deficits via dysregulated eIF4E-dependent translational control. *Nature*. 2013;493(7432):371–7.
50. Cornille M et al. FGFR3 overactivation in the brain is responsible for memory impairments in Crouzon syndrome mouse model. *J Exp Med*. 2022;219(4).
51. Haditsch U, et al. A central role for the small GTPase Rac1 in hippocampal plasticity and spatial learning and memory. *Mol Cell Neurosci*. 2009;41(4):409–19.
52. Shepherd JD, Bear MF. New views of Arc, a master regulator of synaptic plasticity. *Nat Neurosci*. 2011;14(3):279–84.
53. Niekisch H, et al. Learning induces transient upregulation of Brevican in the auditory cortex during consolidation of Long-Term Memories. *J Neurosci*. 2019;39(36):7049–60.
54. Saglam A, Calof AL, Wray S. Novel factor in olfactory ensheathing cell-astrocyte crosstalk: anti-inflammatory protein  $\alpha$ -crystallin B. *Glia*. 2021;69(4):1022–36.
55. Quarles RH. Myelin-associated glycoprotein (MAG): past, present and beyond. *J Neurochem*. 2007;100(6):1431–48.
56. Winocur G, et al. Inhibition of neurogenesis interferes with hippocampus-dependent memory function. *Hippocampus*. 2006;16(3):296–304.
57. Shors TJ, et al. Neurogenesis in the adult is involved in the formation of trace memories. *Nature*. 2001;410(6826):372–6.
58. Kuhn HG, Dickinson-Anson H, Gage FH. Neurogenesis in the dentate gyrus of the adult rat: age-related decrease of neuronal progenitor proliferation. *J Neurosci*. 1996;16(6):2027–33.
59. Drapeau E, et al. Spatial memory performances of aged rats in the water maze predict levels of hippocampal neurogenesis. *Proc Natl Acad Sci U S A*. 2003;100(24):14385–90.
60. Clelland CD, et al. A functional role for adult hippocampal neurogenesis in spatial pattern separation. *Science*. 2009;325(5937):210–3.
61. Klein LR, et al. Intramuscular midazolam, Olanzapine, Ziprasidone, or Haloperidol for treating Acute Agitation in the Emergency Department. *Ann Emerg Med*. 2018;72(4):374–85.
62. Curran HV, Java R. Memory and psychomotor effects of oxcarbazepine in healthy human volunteers. *Eur J Clin Pharmacol*. 1993;44(6):529–33.

## Publisher's Note

Springer Nature remains neutral with regard to jurisdictional claims in published maps and institutional affiliations.